

An Effective Antarctic Ice Surface Temperature Retrieval Method for MODIS

Tingting Liu, Zemin Wang, Xin Huang, Liqin Cao, Muye NIU, and Zhongxiang Tian

Abstract

Given the close relationship between surface melt in polar areas and ice surface temperature (IST), it is important to develop an effective IST retrieval method. However, the studies concerning this topic are relatively limited. In this context, this paper proposes an effective approach to retrieve IST in the Antarctic area by presenting a modified split-window algorithm (SWA) and introducing a polynomial fitting for atmospheric transmittance simulation. The effectiveness was quantitatively validated by a comparative study with a Moderate Resolution Imaging Spectroradiometer (MODIS) IST product (MOD29) and automatic weather station (AWS) data. The comparisons indicated that the proposed method shows a robust performance in Antarctic IST retrieval for MODIS data: the bias was -0.61 K and the root-mean-square error (RMSE) was 1.32 K for the Zhongshan Station data set; the bias was -1.62 K and the RMSE was 2.34 K for the Ross Ice Shelf data set.

Introduction

The study of the polar areas has been the subject of great interest in recent decades, as the polar areas are sensitive to the global environmental change (GEC) and interact closely with many environmental factors in the GEC systems (Wynne and Lillesand, 1993; Peter *et al.*, 1999; Harvey and Green, 2013). Among the various changes in the polar areas, the issue of surface melt deserves special attention and discussion since it contributes to the accelerated disintegration of the ice sheet (Zwally *et al.*, 2002). Surface melt has a direct relationship with surface temperature. Consequently, extracting accurate ice surface temperatures (ISTs) can provide further insight into the process of the surface melt.

Although a lot of automatic weather stations (AWSs) have been established in the polar areas (Steffen *et al.*, 1996; Lazara *et al.*, 2012), they are far from sufficient for IST monitoring in the broad polar areas. Compared with AWS data, remotely sensed imagery can provide fruitful and timely data for Earth observation across both time and space. In particular, the application of thermal infrared (TIR) data can offer a more practical approach to IST information extraction. Recent studies have seen an increasing application of TIR data to land surface temperature (LST) retrieval (Tang *et al.*, 2008; Xiao *et al.*, 2008; Peña, 2009; Nichol, 2009; Rajasekar and Weng, 2009; Jimenez-Munoz *et al.*, 2014).

Tingting Liu, Zemin Wang, and Muye NIU are with the Chinese Antarctic Center of Surveying and Mapping, Wuhan University, 129 Luoyu Road, Wuhan, P.R. China (zmwang@whu.edu.cn).

Xin Huang is with the State Key Laboratory of Information Engineering in Surveying, Mapping and Remote Sensing, Wuhan University, 129 Luoyu Road, Wuhan, P.R. China.

Liqin Cao is with the School of Printing and packaging, Wuhan University, 129 Luoyu Road, Wuhan, P.R. China.

Zhongxiang Tian is with the National Marine Environmental Forecasting Center, 8 Dahuisi Road, Beijing, P.R. China.

Research into TIR-based LST estimation has experienced significant progress in recent decades. Multispectral TIR sensors (e.g., the Moderate Resolution Imaging Spectroradiometer (MODIS)) have gradually replaced other sensors (e.g., the Scanning Multichannel Microwave Radiometer (SMMR) on Nimbus-7 (Comiso, 1994), the Along-Track Scanning Radiometer (ATSR) on ERS-1 (Stroeve *et al.*, 1996), and the Advanced Very High Resolution Radiometer (AVHRR) on NOAA (Leshkevich *et al.*, 1993, Bolgrien *et al.*, 1995; Key *et al.*, 1997; Veihelmann *et al.*, 2001)) as the main data source for LST estimation. Furthermore, the split-window algorithm (SWA) has been found to be an efficient approach for LST estimation. Recently, a few studies have investigated TIR-based IST estimation. Hall *et al.* (2004) proposed a procedure to produce a standard MODIS-based polar sea ice product suite (MOD29). The relationship between melt season IST and the mass balance of Greenland (2000 to 2005) was analyzed in the research of Hall *et al.* (2006). The difference between IST products and AWS data over Greenland was further analyzed by Hall *et al.* (2008), to address the uncertainties and limitations associated with the existing IST products. Other studies have focused on ice surface emissivity (Hori *et al.*, 2006; Hwang *et al.*, 2008), IST and ice extent analysis (Liu *et al.*, 2009; Sobota, 2011; Shu *et al.*, 2012; Hall *et al.*, 2013), IST-based application (Ciappa *et al.*, 2012), and so on. However, an effective IST estimation process for the Antarctic area is still required. Most of the existing SWAs (Coll *et al.*, 1994; Franca and Cracknell, 1994; Thenkabail *et al.*, 2007) require some parameters and coefficients that are difficult to estimate in the real world, since the *in situ* data used to calculate the parameters and coefficients are often quite difficult to obtain in the Antarctic area.

In this paper, to address these shortcomings, an effective SWA-based approach is proposed for IST retrieval in the Antarctic from MODIS data. The notable advantages of the proposed method include the following two aspects:

1. Development of an effective IST estimation method for the Antarctic area. First, the modified SWA developed by Qin *et al.* (2001) is introduced into the IST retrieval, which requires only two parameters (surface emissivity and atmospheric transmittance), without the complicated estimation of other coefficients and parameters. Furthermore, in the procedure of atmospheric transmittance estimation, the relationship between water vapor and atmospheric transmittance is simulated by a series of polynomial functions, replacing the traditional linear fitting.
2. Validation of the proposed method based on AWS data. Although Qin's method (2001) has been successfully used in many areas (Mao *et al.*, 2005), its effectiveness in the polar areas has not yet been verified. For this purpose, in this study, the method is modified and

Photogrammetric Engineering & Remote Sensing
Vol. 81, No. 11, November 2015, pp. 861–872.
0099-1112/15/861–872

© 2015 American Society for Photogrammetry
and Remote Sensing
doi: 10.14358/PERS.81.11.861

extended to application in the Antarctic. Based on the AWS data (from Zhongshan Station and the Ross Ice Shelf), a comparison between the retrieved IST results and the MOD29 product is conducted.

The rest of this paper is organized as follows. The experimental data and study areas are described in the next Section, followed by theoretical aspects of the proposed processing chain, including the SWA, the emissivity, and atmospheric transmittance estimation. The next Section presents the algorithm validation and the experimental results, comparisons, and discussion, followed by the Conclusions.

Data Source

Satellite Data

The MODIS radiometer is operational onboard the polar orbiting Terra and Aqua satellites of the NASA Earth Observing System (EOS). It has a viewing swath width of 2,330 km and covers most of the Earth's surface within several days. The satellite data products used in this research came from the MODIS radiometer. The general information about these data products is summarized in Table 1.

The TIR bands used to retrieve the IST in this research were derived from the MODIS L1b data (MOD021KM). MOD021KM has 36 spectral bands between 0.405 and 14.385 μm , among which the infrared bands 31 and 32 (centered on 11.03 and 12.02 μm , respectively) were used to retrieve the IST. The ground resolution of these two bands is 1 km. The MODIS geolocation data (MOD03) were used to reproject the MOD021KM data. In addition, a MODIS cloud mask product (MOD35_L2) was employed to remove cloud pixels in the MOD021KM data.

However, the accuracy of MOD35_L2 is limited. Improvement of this product has been implemented, reducing the misidentification of cloud as clear to 16.3 percent, but the improvement does not change the misidentification of clear as cloud (Hall *et al.*, 2012; Liu *et al.*, 2004; Frey *et al.*, 2008)). Moreover, a further comparison (Liu *et al.*, 2010) showed that the MOD35 product performs better over open water than over sea ice.

The MOD29 product was used to evaluate the accuracy of the proposed method by comparing it with the retrieved IST results. This product, which is generated using the MODIS L1b data, the geolocation product, and the cloud mask product, contains the sea ice extent product, the IST product, and so on.

In Situ Data

In this research, *in situ* data (air temperature and wind speed) from AWSS were used as reference. The two sets of *in situ* data are plotted collectively in Plate 1. One set was provided by the weather station located at Zhongshan Station, which is the second Chinese Antarctic research expedition station. The detailed location of this weather station is 69°22'S / 76°22'E (the red star in Plate 1), on the Larsemann Hills, Prydz Bay, East Antarctica. The other set was provided by the AWSS from the

TABLE 1. THE MODIS DATA PRODUCTS USED IN THIS RESEARCH

Product	Resolution	Used bands	Application
MOD021KM	1 km	Band 2, Band 19, Band 31, Band 32	IST retrieval using the proposed method
MOD03	1 km	Band 1	Calibration for MOD021KM
MOD35_L2	1 km	Band 1	Cloud pixel removal for MOD021KM
MOD29	1 km	Band 2	Algorithm validation

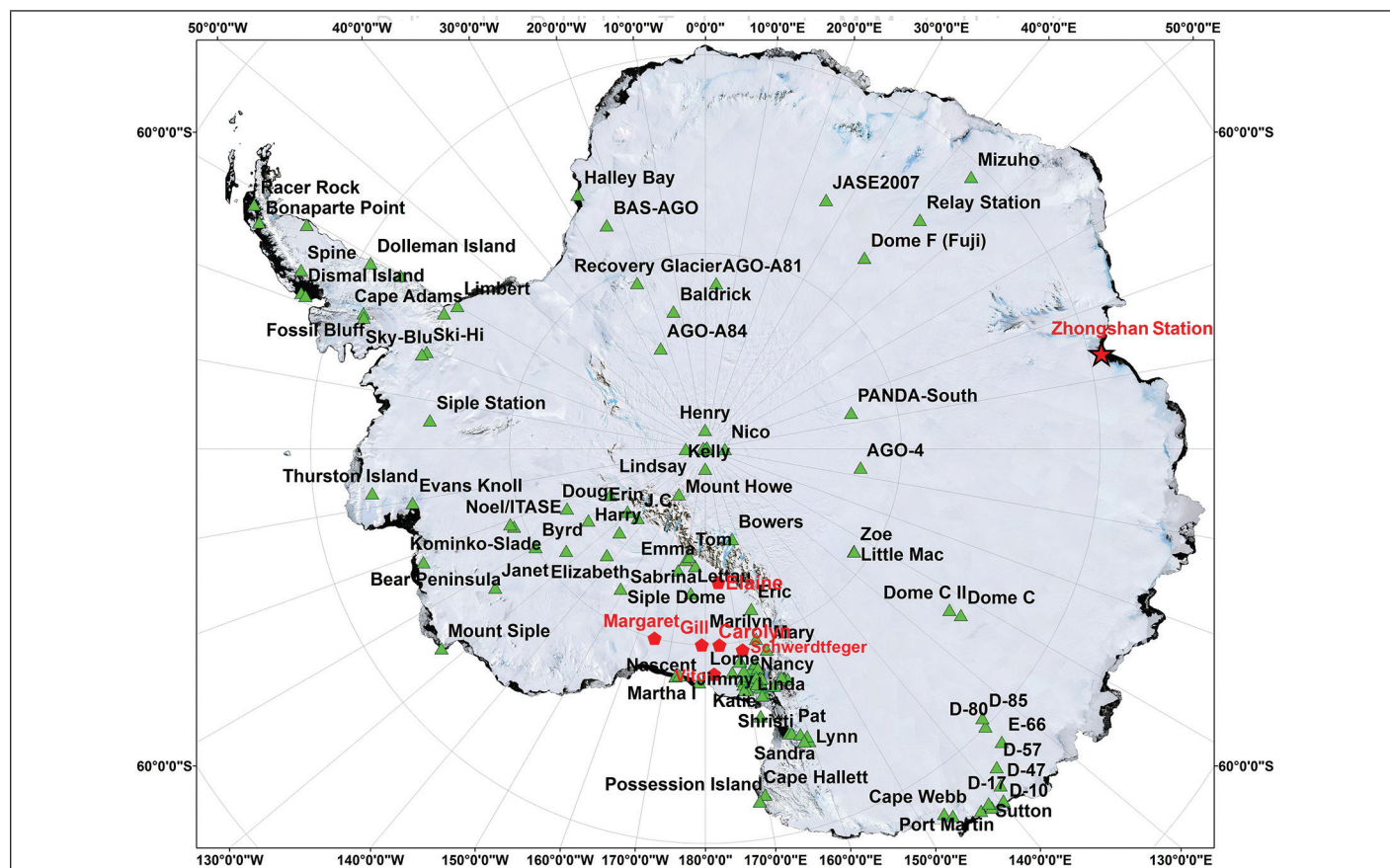


Plate 1. Automatic weather stations located in the Antarctic area. The stations used in this research are shown in red, with the Zhongshan Station AWS marked by a red star and the Ross Ice Shelf AWSs marked by red dots. The green triangles show the other AWSs from the AMRC and the AWS program.

Antarctic Meteorological Research Center (AMRC) and the AWS program (AMRC and AWS, 2014). To date, 133 AWSS have been built in the Antarctic as part of this program. The locations of these AWSS are shown in Plate 1, marked by green triangles and red dots. In this Plate, the red dots and red star represent the stations considered in this study, and the corresponding data were used as references for the method validation.

Experimental Data Selection

Only data acquired from the ice shelf were used in the experiments, since the MOD29 and MOD35 products are available for the polar sea ice, Greenland, and the ice shelf in the Antarctic, but unavailable for the Antarctic ice sheet. The Ross Ice Shelf is one of the biggest ice shelves in the Antarctic. The pixels in satellite images covering this region can therefore be regarded as pure pixels. Taking this factor into account, comparisons were conducted using AWS data from the Ross Ice Shelf. In the experiments, 165 cloud-free scenes from December 2004 to December 2013 were chosen, with several instances shown in Figure 1.

Additional experiments were conducted using the weather station data from Zhongshan Station. In this part, 33 scenes identified as cloud free by MOD35 during December 2004 and December 2013 were chosen, six of which are shown in Figure 2.

Due to the particularity of the Antarctic climate and the impact of the polar night, only images from the summer were used to retrieve the IST.

The AWS data are sometimes uncertain. Under clear sky conditions, the temperature sensor can overheat when the downward solar irradiance exceeds 240 Wm^{-2} and the wind speed is less than 4 ms^{-1} (Hudson *et al.*, 2005; Hall *et al.*, 2008; Shuman *et al.*, 2014). Strong winds can, however, suppress this effect. Thus, in this research, the acquired air temperature values were not considered if the wind speed was less than 4 ms^{-1} . It should be noted that all the MODIS-based IST values (retrieved results and MOD29 product) correspond to the location and time of the AWS measurements.

Methods

The theoretical basis for satellite-image-based LST is that the total radiance emitted by the ground increases rapidly with the increase in temperature (Qin *et al.*, 2001). Although much effort has been devoted to retrieving LST from remotely sensed imagery, this study proposes an effective approach for Antarctic IST retrieval. The flowchart of the proposed MODIS-based IST retrieval method is shown in Figure 3.

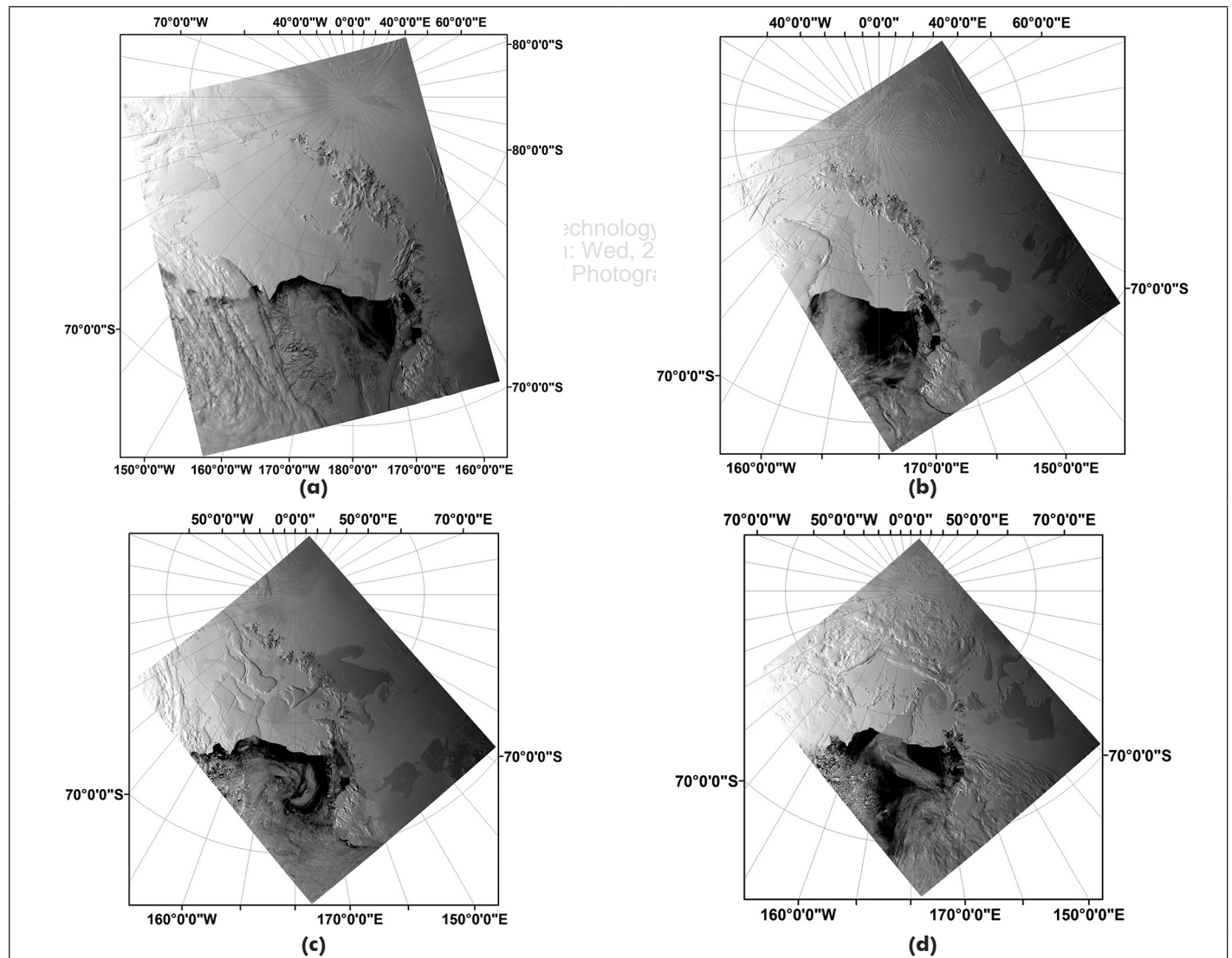


Figure 1. Four scenes of the MOD021KM data from the Ross Ice Shelf. The number of each scene consists of two parts, the year and the Julian Day Number: “2013” is the year; “339,” “335,” “342,” and “358” are the Julian Day Numbers: (a) 01 December 2013 (No. 2013-335), (b) 05 December 2013 (No. 2013-339), (c) 08 December 2013 (No. 2013-342), and (d) 24 December 2013 (No. 2013-358).

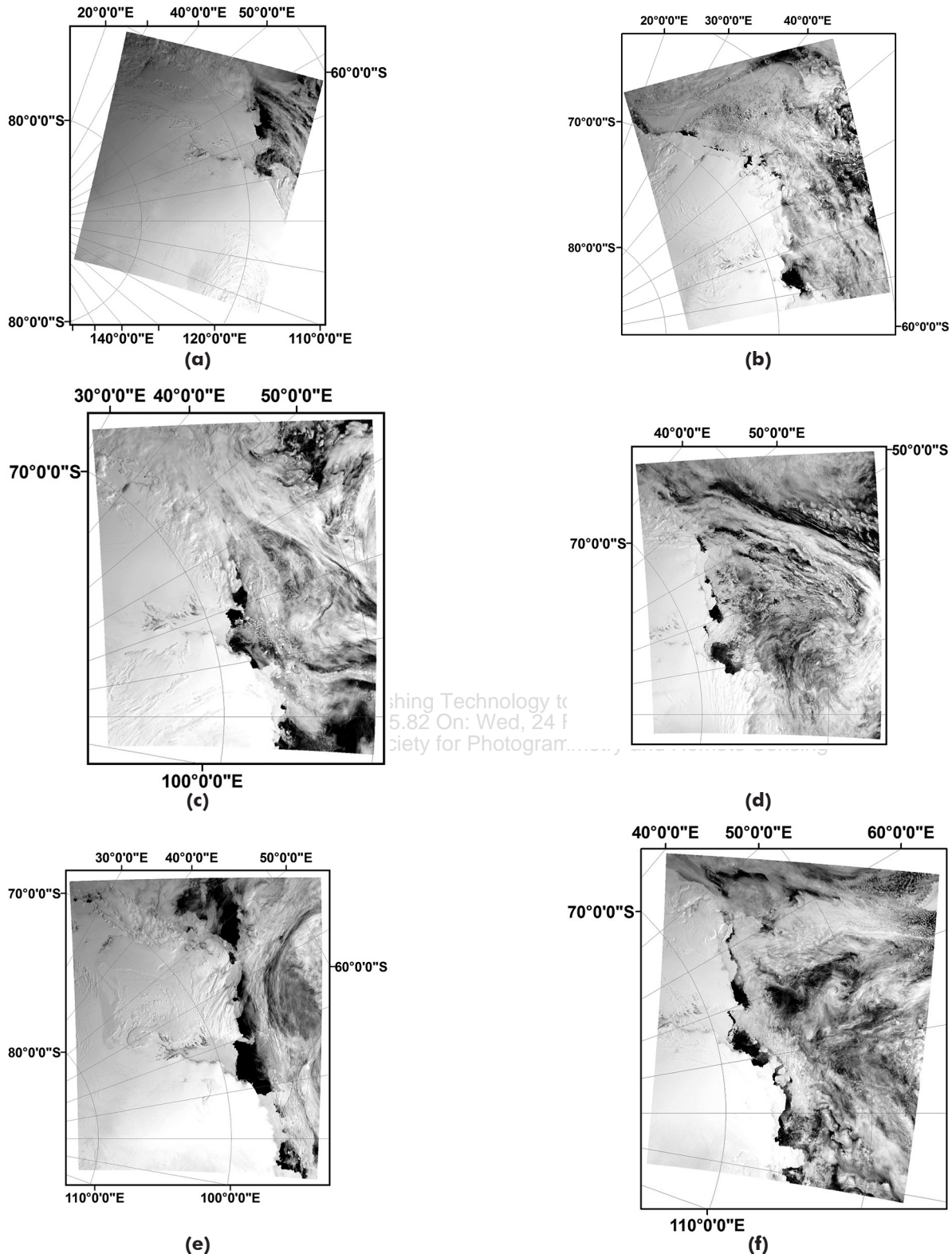


Figure 2. Six scenes of the MOD021KM data from Zhongshan Station. The number of each scene consists of two parts, the year and the Julian Day Number: “2008,” “2009,” “2010,” “2011,” “2012,” and “2013” are the years; “339,” “335,” “342,” and “358” are the Julian Day Numbers: (a) 09 December 2008 (No. 2008-344), (b) 01 December 2009 (No. 2009-335), (c) 12 December 2010 (No. 2010-346), (d) 06 December 2011 (No. 2011-340), (e) 27 December 2012 (No. 2012-361), and (f) 24 December 2013 (No. 2013-358)

Split-Window Algorithm Theory

The SWA is one of the multichannel LST retrieval methods. Its principle is based on the relationship between the radiance and temperature in the two infrared windows (the 11 to 12 μm

atmospheric window) for a given temperature. It was first proposed by McMillin (1975), and was initially used to retrieve sea surface temperature (SST). The SWA has also been further modified for SST retrieval (McClain *et al.*, 1985; Barton *et al.*, 1989;

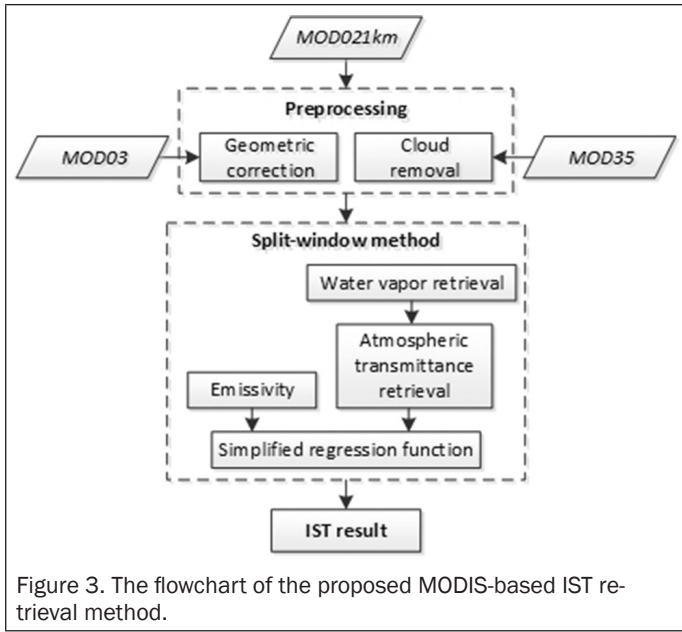


Figure 3. The flowchart of the proposed MODIS-based IST retrieval method.

Niclòs *et al.*, 2007; Vincent, 2000) and LST retrieval (Price, 1984; Tang *et al.*, 2008; Xiao *et al.*, 2008; Peña, 2009; Nichol, 2009; Rajasekar and Weng, 2009; Jimenez-Munoz *et al.*, 2014).

The SWA used in the MOD29 retrieval procedure is implemented as a regression model, which can be described as the following equation (Hall *et al.*, 2004):

$$T_s = a + bT_{31} + c(T_{31} - T_{32}) + d[(T_{31} - T_{32})(\sec\theta - 1)] \quad (1)$$

where T_s is the surface temperature; T_{31} and T_{32} are the brightness temperatures of bands 31 and 32 in the MOD021KM data, respectively; θ is the sensor scan angle; and a , b , c , and d are the regression coefficients. In this procedure, large quantities of *in situ* data are used to determine the empirical relationship and its corresponding coefficients in Equation 1 through a least squares regression method.

In this research, an improved SWA was used to implement the MODIS-based IST retrieval in the Antarctic area. This improved version of SWA, which was developed by Qin *et al.* (2001), requires only two essential parameters (emissivity and transmittance), and can be described as the following simple regression function:

$$T_s = A_0 + A_1 T_{31} - A_2 T_{32} \quad (2)$$

where A_0 , A_1 , and A_2 are the coefficients, which are determined by the atmospheric transmittance, the ground emissivity, and viewing angle:

$$A_0 = \frac{a_{31}D_{32}(1-C_{31}-D_{31})}{(D_{32}C_{31}-D_{31}C_{32})} - \frac{a_{32}D_{31}(1-C_{32}-D_{32})}{(D_{32}C_{31}-D_{31}C_{32})} \quad (3)$$

$$A_1 = 1 + \frac{D_{31}}{(D_{32}C_{31}-D_{31}C_{32})} - \frac{b_{31}D_{32}(1-C_{31}-D_{31})}{(D_{32}C_{31}-D_{31}C_{32})} \quad (4)$$

$$A_2 = \frac{D_{31}}{(D_{32}C_{31}-D_{31}C_{32})} + \frac{b_{32}D_{31}(1-C_{32}-D_{32})}{(D_{32}C_{31}-D_{31}C_{32})} \quad (5)$$

where $a_{31}=-64.60363$, $b_{31}=0.440817$, $a_{32}=-68.72575$, $b_{32}=0.473453$, and

$$C_i = \varepsilon_i \tau_i(\theta) \quad (6)$$

$$D_i = [1 - \tau_i(\theta)][1 + (1 - \varepsilon_i) \tau_i(\theta)] \quad (7)$$

where $\tau_i(\theta)$ is the atmospheric transmittance of the i^{th} band ($i = 31, 32$) on the sensor scan angle θ , and ε_i is the surface emissivity of the i^{th} band ($i = 31, 32$).

Equations 6 and 7 indicate that the key steps in this method refer to emissivity acquisition and transmittance estimation. This makes it easier to retrieve IST without the complicated estimation of other coefficients and parameters.

Surface Emissivity

Surface emissivity is defined as the ratio of the radiant energy of an object to the radiant energy of a standard black body at the same temperature. It reflects the different physical characteristics of different land-cover types. Ice/snow surface emissivity is a key parameter for IST retrieval (Warren, 1982; Key and Haeffliger, 1992). Several spectral libraries are available for various types of terrestrial surface emissivity, such as the ASTER (the Advanced Spaceborne Thermal Emission Reflection Radiometer) Spectral Library (Baldrige *et al.*, 1999) and the MODIS UCSB (University of California, Santa Barbara) Emissivity Library (Wan *et al.*, 1994). A number of field campaigns have also been carried out to measure ice/snow emissivity (Hori *et al.*, 2006; Key and Haeffliger, 1992). Emissivity varies with ice/snow surface conditions, such as surface melt (Hori *et al.*, 2006; Salisbury *et al.*, 1994; Wald, 1994), snow grain size (Stroeve *et al.*, 1996), and sensor scan angle (Key and Haeffliger, 1992; Hori *et al.*, 2006). According to Stroeve *et al.* (1996), a 0.1 percent bias in emissivity corresponds to a 0.1 K deviation in IST. In this study, the emissivity over the Antarctic was set to 0.993 (for band 31) and 0.990 (for band 32), referring to the research of Hall *et al.* (2008).

Atmospheric Transmittance

Atmospheric transmittance describes the magnitude of the thermal radiation (TR) attenuation. Attenuation occurs under the influence of the atmospheric constituents and atmospheric scattering when the TR is transferred to sensors. The atmospheric constituents, such as N_2 , O_3 , and CO_2 , are relatively stable; therefore, their influences can be assumed to be constant and can be simulated by the standard atmospheric profiles (Qin *et al.*, 2001). Aerosols can result in atmospheric scattering, but their influence on TR transfer is insignificant considering their low level in the atmosphere. In contrast, water vapor significantly contributes to TR attenuation. The variance of atmospheric transmittance depends on the dynamic of the water vapor content in the standard atmospheric profiles. Therefore, atmospheric transmittance can be estimated by simulating its relationship with water vapor content.

Water Vapor Retrieval

Various approaches (Chesters *et al.*, 1983; Kleespies and McMillin, 1990; Birkenheuer, 1991) have been proposed for water vapor retrieval. The satellite-data-based approaches focus on the absorption of water vapor when the reflected solar radiance is transferred down to the land surface and up through the atmosphere (Kaufman and Gao, 1992). In Kaufman's research (1992), the relationship between transmittance (τ_w) and the total precipitable water vapor (w) was defined as the ratio of several bands. This principle is based on the difference between the atmospheric absorption and the atmospheric window. In this study, a two-band ratio approach was applied:

$$\tau_w = r_i / r_j \quad (8)$$

where r_i is the reflectance of band 19, which is the absorption band; and r_j is the reflectance of band 2, which is the window band. The relationship between the transmittance and the total precipitable water vapor (w) can be expressed using an exponential equation:

$$w = ((\alpha - \ln\tau_w)/\beta)^2, R^2 = 0.999 \quad (9)$$

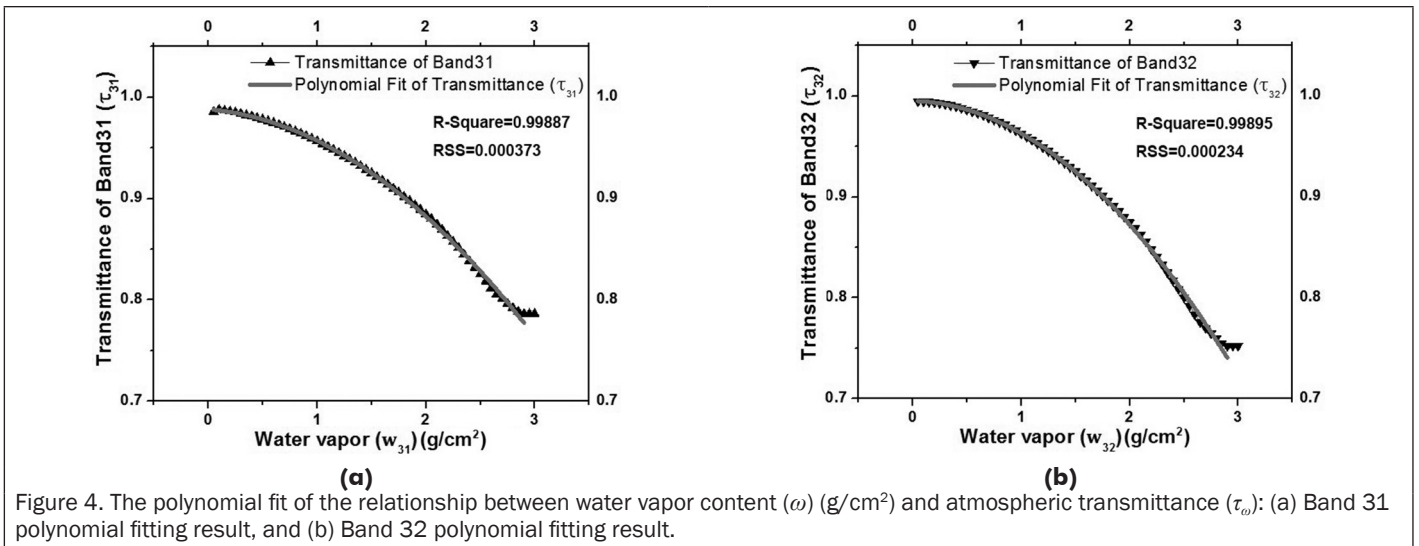


Figure 4. The polynomial fit of the relationship between water vapor content (ω) (g/cm^2) and atmospheric transmittance (τ_ω): (a) Band 31 polynomial fitting result, and (b) Band 32 polynomial fitting result.

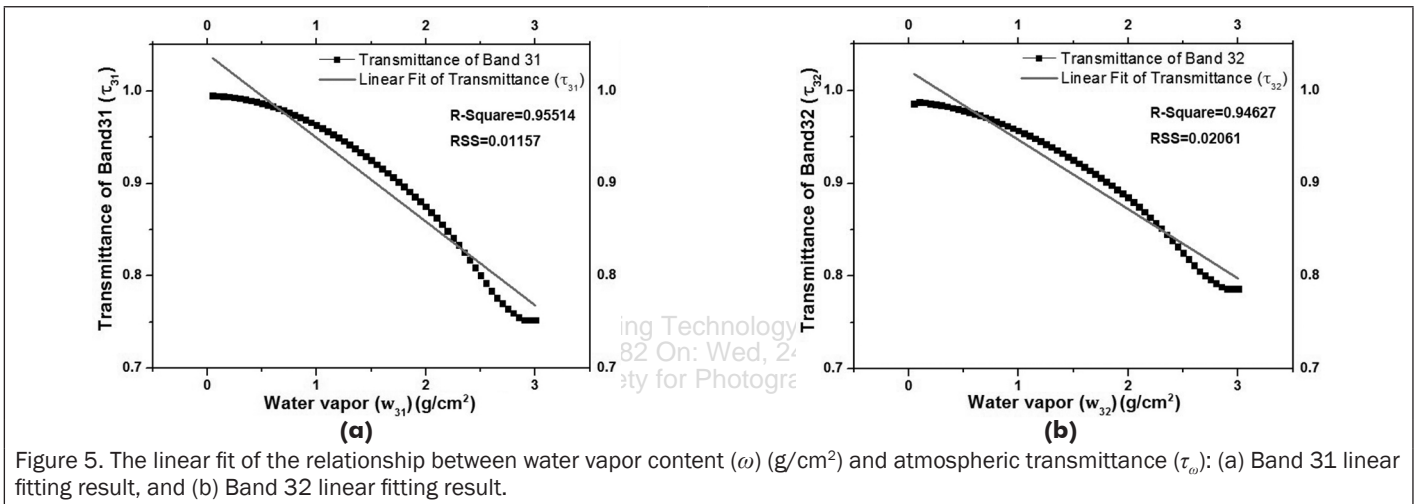


Figure 5. The linear fit of the relationship between water vapor content (ω) (g/cm^2) and atmospheric transmittance (τ_ω): (a) Band 31 linear fitting result, and (b) Band 32 linear fitting result.

where R^2 is the determination coefficient indicating the accuracy of the method, with $R^2 = 0.95514$ and $R^2 = 0.94627$. The two-band ratio method makes it easier to retrieve water vapor content from satellite images without any *in situ* data or simulated coefficients.

Simulation of the Relationship between Water Vapor and Atmospheric Transmittance

It is difficult to directly estimate atmospheric transmittance from satellite data or other atmospheric data. In general, atmospheric transmittance is acquired through simulation using local atmospheric data, especially water vapor content. Simulation of the relationship between atmospheric transmittance and water vapor can be built through atmospheric modeling programs such as MODerate resolution atmospheric TRANsmission (MODTRAN). MODTRAN (Berk *et al.*, 2006) is a “narrow band model” atmospheric radiative transfer program, and its spectral range extends from the ultraviolet into the far-infrared ($0 \sim 50000 \text{ cm}^{-1}$), with a spectral resolution of up to 0.2 cm^{-1} .

In the Antarctic, the volume of water vapor is much lower than other regions, and it contributes little to the annual precipitation. According to the observation data, the minimum and maximum values of water vapor were set as $0.05 \text{ g}/\text{cm}^2$ and $3.0 \text{ g}/\text{cm}^2$, respectively. For this range of water vapor content, the relationship between water vapor content and atmospheric content is approximately nonlinear. Thus, a series of polynomial fitting functions were used to describe the relationship between transmittance and water vapor, replacing the traditional linear fitting. Please see the next Section for more details.

Results and Discussion

Algorithm Validation

The fitting results of the relationship between water vapor content and atmospheric transmittance are presented in Figure 4.

In Figure 4a and 4b, the dotted lines show the change trend of the atmospheric transmittance with the increase in water vapor in the two MODIS thermal channels, bands 31 and 32, respectively. As the water vapor increases, the atmospheric transmittance decreases sharply. Within this range, water vapor has presented a linear relationship with atmospheric transmittance in most of the previous studies (Qin *et al.*, 2001; Mao *et al.*, 2005). However, in this study, it was found that this relationship can be better represented by a polynomial function. The solid lines in Figure 4 a and 4b show the results of polynomial fitting, and the corresponding polynomial equations are provided as follows:

$$\tau_{31} = 0.9955 - 0.00299 \times w_{31} - 0.02926 \times w_{31}^2 \quad (9)$$

$$\tau_{32} = 0.98822 - 0.00902 \times w_{32} - 0.02193 \times w_{32}^2 \quad (9)$$

In Figure 4, higher determination coefficients (R^2) correspond to more accurate results. A small value for the residual sum of squares (RSS) also indicates a relatively high accuracy. The accuracy for the linear-fitting-based regression analysis and the fitting results are provided in Figure 5.

The lower accuracy and the linear fitting results in Figure 5 indicate that the linear fitting cannot accurately describe the

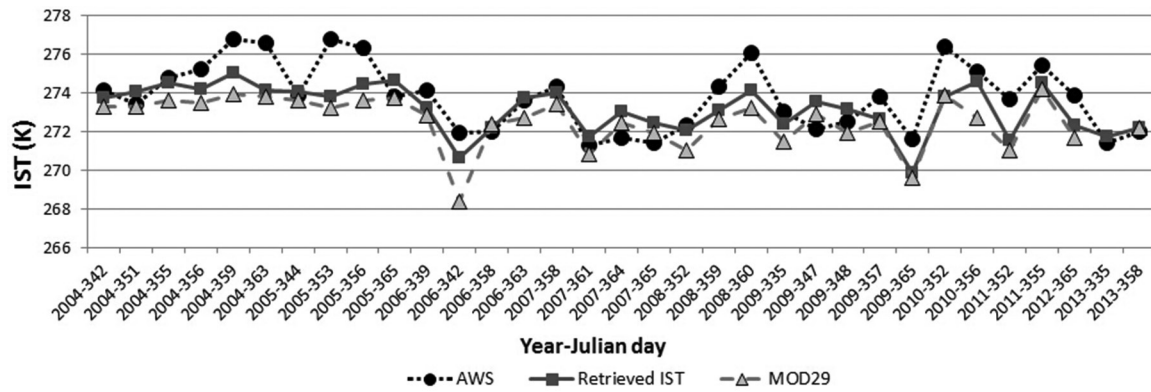


Figure 6. A comparison of satellite-derived ISTs (retrieved IST and MOD29 product) and *in situ* AWS ISTs from Zhongshan Station. From December 2004 to December 2013, 33 cloud-free scenes with a corresponding wind speed of greater than 4 ms^{-1} were chosen for the comparison.

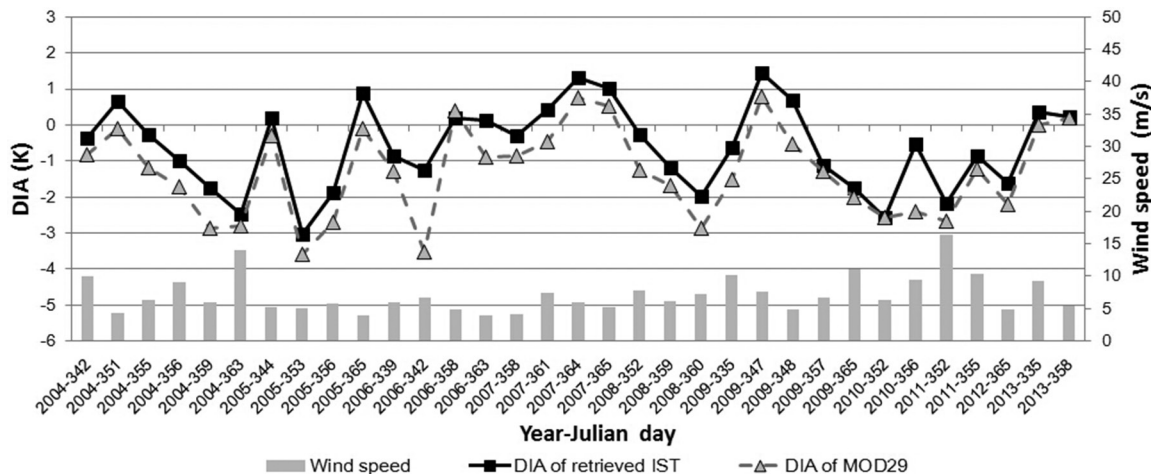


Figure 7. The differences between the air temperature and the retrieved IST, and those between the air temperature and the MOD29 product, for Zhongshan Station.

TABLE 2. THE ACCURACY OF THE RETRIEVED IST AND THE MOD29 PRODUCT FOR ZHONGSHAN STATION

Data	Accuracy	
	Bias (K)	RMSE (K)
Retrieved IST	-0.62	1.32
MOD29	-1.34	1.81

TABLE 3. THE EIGHT SCENES WITH THE GREATEST DIFFERENCE (ABSOLUTE VALUE) VALUES. IT WAS EVALUATED THROUGH VISUAL INTERPRETATION WHETHER EACH SCENE WAS IMPACTED BY FOG/CLOUD

Number	The differences between the air temperature and the retrieved IST (K)	The differences between the air temperature and the MOD29 (K)	Comments
2004-359	-1.76	-2.87	Fog/cloud
2004-363	-2.48	-2.82	Fog/cloud
2005-353	-3.02	-3.58	Fog/cloud
2008-360	-1.98	-2.87	Fog/cloud
2009-365	-1.74	-2.02	Clear
2010-352	-2.59	-2.56	Fog/cloud
2011-352	-2.18	-2.67	Fog/cloud
2012-365	-1.61	-2.2	Clear

relationship between water vapor and atmospheric transmittance. In contrast, the polynomial fitting can better describe this relationship.

Comparison

The retrieved IST obtained by the proposed method was compared with the MOD29 product and the AWS data. The first comparison was conducted based on the data from Zhongshan Station (Figure 6). This figure presents the results of the retrieved IST, the MOD29 product, and the AWS data.

Referring to the AWS data, the bias and root-mean-square error (RMSE) for the retrieved IST and the MOD29 product are provided in Table 2.

The retrieved IST exhibits a much higher accuracy than the MOD29 product. In addition, the differences between the air temperature and the retrieved IST, and those between the air temperature and the MOD29 product, are presented in Figure 7.

In Figure 7, the difference (absolute value) values of eight sets of samples are much higher than those of the others (Table 3). After visual interpretation by employing MOD021KM data, it was found that two of these scenes were clear and six scenes were affected by suspected fog or cloud. Taking these six scenes out of the calculation, the revised bias and RMSE are reported in Table 4. The accurate results imply that the precision of the results is related to the precision of the MOD35 product. However, it is difficult to determine the accuracy of the MOD35 product due to the similar spectral characteristics between cloud and snow/ice.

Hall *et al.* (2004) found that the differences were slightly greater when wind speeds were lower, and were less when

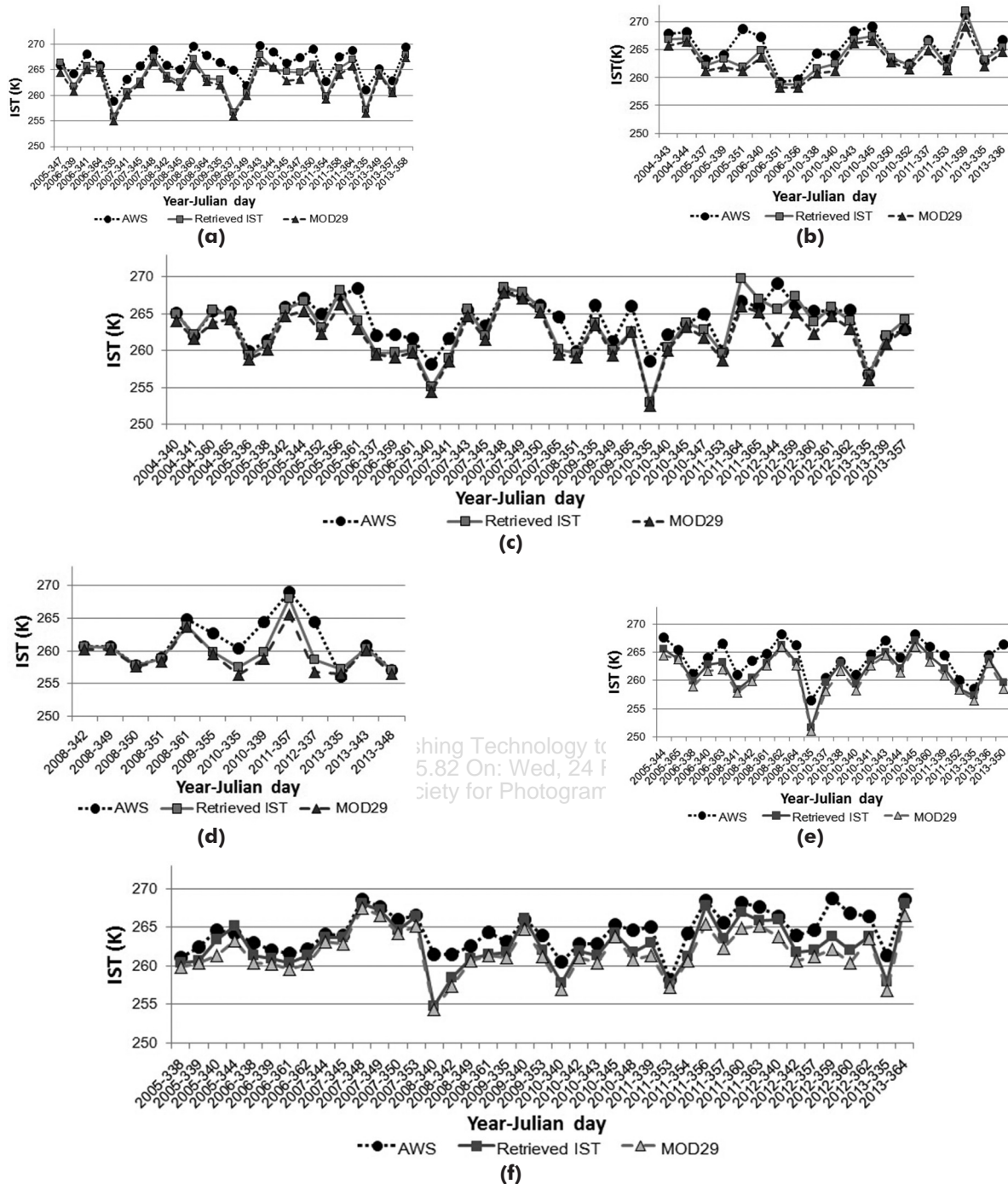


Figure 8. Comparison of satellite-derived ISTs (retrieved IST and MOD29 product) and *in situ* AWS ISTs for the Ross Ice Shelf. From December 2004 to December 2013, 165 cloud-free scenes with a corresponding wind speed of greater than 4 ms⁻¹ were chosen for the comparison: (a) Carolyn AWS, (b) Elaine AWS, (c) Gill AWS, (d) Margaret AWS, (e) Schwerdtfeger AWS, and (f) Vito AWS

TABLE 4. THE ACCURACY OF THE RETRIEVED IST AND THE MOD29 PRODUCT FOR ZHONGSHAN STATION, WITHOUT THE SIX SCENES LISTED IN TABLE 3 AS "FOG/CLOUD"

Data	Accuracy	
	Bias (K)	RMSE (K)
Retrieved IST	-0.24	0.94
MOD29	-0.98	1.45

TABLE 5. PEARSON'S CORRELATION COEFFICIENTS BETWEEN WIND SPEED AND THE DIFFERENCES BETWEEN THE AIR TEMPERATURE AND THE RETRIEVED IST/MOD29 PRODUCT FOR ZHONGSHAN STATION (N = 33)

	The differences between the air temperature and the retrieved IST	The differences between the air temperature and the MOD29
Wind speed	-0.368*	-0.352*

*P<0.05; ns: no significant correlation.

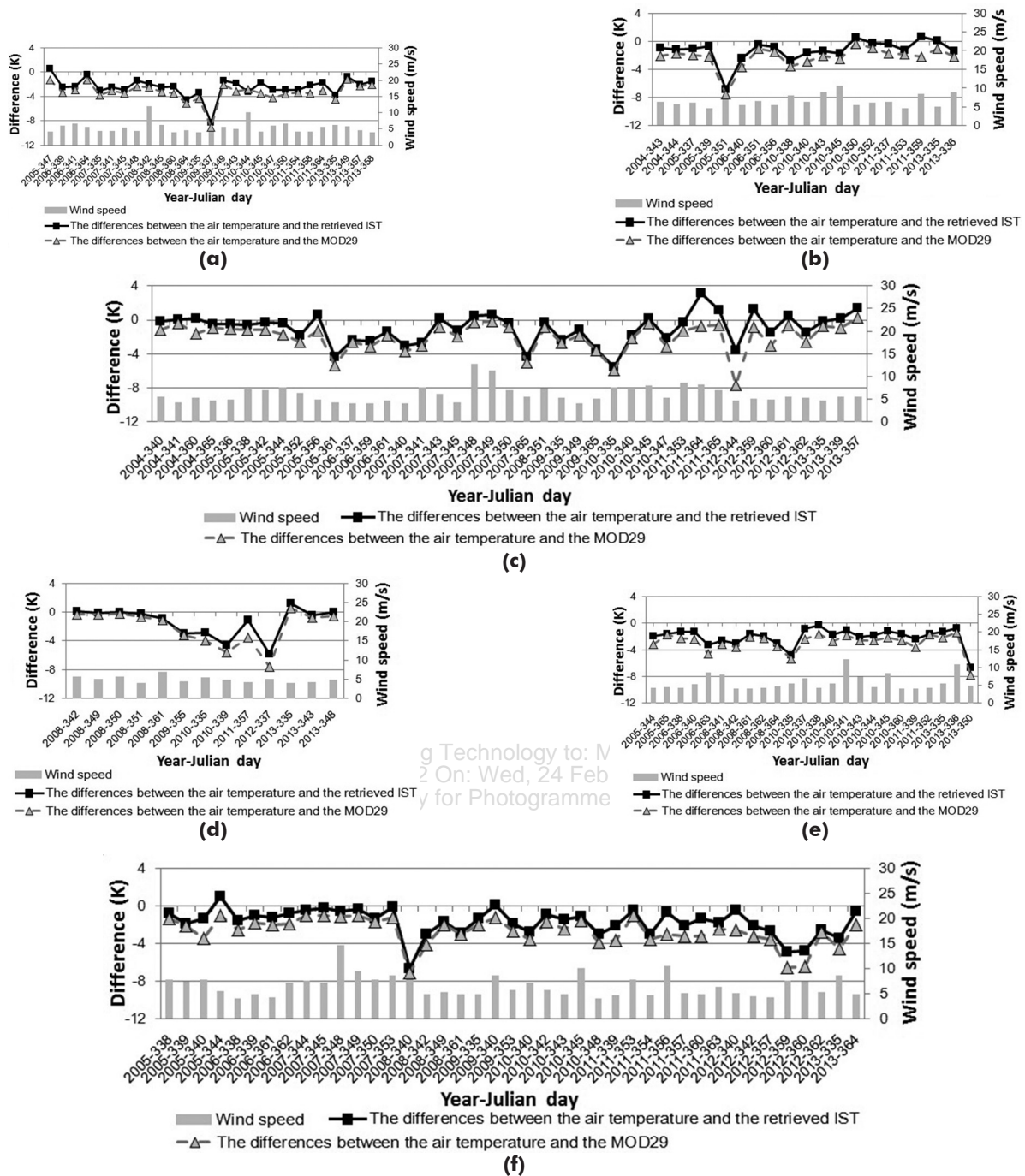


Figure 9. The differences between the air temperature and the retrieved IST, and those between the air temperature and the MOD29 product, for the Ross Ice Shelf: (a) Carolyn AWS, (b) Elaine AWS, (c) Gill AWS, (d) Margaret AWS, (e) Schwerdtfeger AWS, and (f) Vito AWS.

wind speeds were higher. Thus, the wind speed data were utilized in the experiment, as shown in Figure 7, to determine whether the wind speed affected the differences between the air temperature and the retrieved IST/MOD29 product in this research. A statistical analysis of the correlation between wind speed and the differences between the air temperature and the retrieved IST/MOD29 product is summarized in Table 5.

The Pearson's correlation coefficients give a value between 1 and -1, where 1 and -1 indicate totally positive and negative correlation, respectively, and 0 indicates no correlation. In Table 5, the results show that the differences between the air temperature and the retrieved IST/MOD29 product were both positively correlated with wind speed.

In the above experiments, the proposed method exhibited a better IST retrieval performance for the Zhongshan Station data. Similar experiments were implemented using the MODIS-based results and the AWS observation data from the Ross Ice Shelf. The results are shown in Figure 8.

The differences between the air temperature and the retrieved IST, and those between the air temperature and the MOD29 product, for each AWS, are presented in Figure 9.

According to Figures 8 and 9, the retrieved ISTs and the MOD29 product present a better agreement than the AWS ISTs. The corresponding accuracy of these experiments is summarized in Table 6.

The improvement in accuracy achieved by the retrieved IST results can be clearly observed in this table. The wind speed

TABLE 6. THE ACCURACY OF THE RETRIEVED ISTS AND THE MOD29 PRODUCT FOR THE SIX AWSs ON THE ROSS ICE SHELF

	Data	AWSs					
		Carolyn	Elaine	Gill	Margaret	Schwerdtfeger	Vito
Bias (K)	Retrieved IST	-2.46	-1.26	-0.98	-1.35	-2.07	-1.70
	MOD29	-3.27	-2.27	-1.97	-2.10	-2.89	-2.69
RMSE (K)	Retrieved IST	2.91	2.02	2.01	2.40	2.47	2.44
	MOD29	3.59	2.72	2.60	3.17	3.21	3.49

values obtained during the same period are also presented in Figure 9. The statistical analysis results, showing the correlations between wind speed and the differences between the air temperature and the retrieved IST/MOD29 product, are summarized in Table 7, where no significant correlation is observed. This implies that the difference between IST and air temperature was not impacted by wind speed.

Discussion

According to the experiments, an immediate conclusion is that the proposed method generates a higher accuracy than the MOD29. A further analysis follows.

Most of the available *in situ* records of air temperature in polar areas are from AWSs. In consideration of the cost and the power consumption, thermistors and passive shields are used in AWSs, both of which have been shown to be significantly affected by high solar radiation and low wind speeds (Genthon *et al.*, 2011). According to some researchers (Hudson *et al.*, 2005; Hall *et al.*, 2008; Genthon *et al.*, 2011; Shuman *et al.*, 2014), this uncertainty usually occurs when the downward solar irradiance exceeds 240 Wm^{-2} and the wind speed is less than 4 ms^{-1} . This effect cannot be easily corrected since it is shield dependent. Therefore, only air temperature values acquired when the wind speed was greater than 4 ms^{-1} were considered in this research.

The biases in Tables 2, 4, and 6 were calculated using mean values, which represent the deviation of the MODIS-based IST from *in situ* records. The biases of the retrieved ISTs were $0.72 \sim 0.92 \text{ K}$ less than for the MOD29 product, indicating that the retrieved ISTs were accurate. The biases, which are not presented in the above comparisons, were also calculated for all the data from Zhongshan Station and the Ross Ice Shelf (-1.46 K for the retrieved IST and -2.34 K for the MOD29 product). The negative bias indicates that the MODIS-based IST is lower than the *in situ* air temperature. This is mostly due to the difference between the surface and air temperature, which commonly exists in the presence of atmospheric temperature inversion (Marks, 2002). This bias is consistent with the findings of Hall *et al.* (2008), where the MODIS-based LSTs were -2 K lower than the AWS-derived air temperatures. Furthermore, Koenig and Hall (2010) found a -3 K bias, and Shuman *et al.* (2014) found a -5 K bias.

However, some instances (see Figures 7 and 9) indicate that the MODIS-derived IST is slightly higher than the corresponding air temperature. Referring to Miller's research (1956), this phenomenon is probably caused by the mixing of warmer air from aloft during storms, which was also mentioned in Hudson and Brandt (2005). Furthermore, clouds are another aspect that can make the surface warmer, in that they have a scattering effect on radiation transfer in the atmosphere, which can affect the incoming solar radiation.

Although the difference between the MODIS-derived ISTs and the observation-based records is clear, the proposed method presents a better performance than MOD29. This can be attributed to the application of polynomial fitting in analyzing the relationship between water vapor and atmospheric transmittance. A similar conclusion was also presented in Ouaidrari's research (2002), in which a quadratic split-window equation provided better accuracy than a linear split-window equation for AVHRR-derived LST.

TABLE 7. PEARSON'S CORRELATION COEFFICIENTS BETWEEN WIND SPEED AND THE DIFFERENCES BETWEEN THE AIR TEMPERATURE AND THE RETRIEVED IST/MOD29 PRODUCT, FOR THE ROSS ICE SHELF (N = 165)

	The differences between the air temperature and the retrieved IST	The differences between the air temperature and the MOD29
Wind speed	ns	ns

ns: no significant correlation.

A limitation of this method is that its accuracy is affected by clouds or fog. The accuracy of the IST retrieval method therefore relies on the accuracy of the cloud detection result. Even though there have been effective methods developed for cloud detection (Liu *et al.*, 2004; Frey *et al.*, 2008), they are extremely difficult to apply in the polar areas. The similar spectral reflectance between cloud and ice/snow makes it difficult to automatically identify cloud; therefore, it is not easy to determine whether the weather condition is "cloud free" or "cloudy." As a result, some studies have relied on passive-microwave-derived IST to solve this problem associated with optical data (Cavalieri, 1984; Germain and Cavalieri, 1997; Cavalieri, 1994). However, the IST retrieval accuracy from passive microwave data is unstable since the emissivity is variable, depending on the ice/snow conditions (such as melt or dry) (Mcfarland *et al.*, 1990).

Conclusions

This paper has proposed an approach to retrieve ice surface temperature (IST) in the Antarctic region, based on a modified split-window algorithm (SWA) and atmospheric transmittance estimation. Through a MODTRAN simulation and regression analysis, we propose to build the relationship between atmospheric transmittance and water vapor using a polynomial form, replacing the traditional linear fitting. In this way, more accurate results were obtained in our experiments. The effectiveness was quantified by a comparison with the MOD29 product and AWS data from Zhongshan Station and the Ross Ice Shelf from 2004 to 2013. The results showed that the proposed method can generate a higher accuracy than the MOD29 product. In addition, the influence of wind speed on the differences between IST and air temperature was characterized, with a correlation between wind speed and the differences observed for Zhongshan Station, but no significant correlation found for the Ross Ice Shelf. Overall, our study is able to provide technical support and a processing framework for Antarctic surface melt detection.

Acknowledgments

This research was supported by the projects: the National Natural Science Foundation of China (41206177 and 91338111); the National High Technology Research and Development Program of China (863 program) (2012AA12A304, 2013AA12A301); and the Fundamental Research Funds for the Central Universities (2042014kf0293).

References

- AMRC and AWS, 2015. URL: <http://amrc.ssec.wisc.edu/aboutus/> (last date accessed: 23 September 2015).
- Baldrige, A.M., S.J. Hook, C.I. Grove, and G. Rivera, 2009. The ASTER spectral library version 2.0, *Remote Sensing of Environment*, 113(4):711–715.
- Barton, I.J., A.M. Zavody, D.M. O'Brien, D.R. Cutten, R.W. Saunders, and D.T. Llewellyn-Jones, 1989. Theoretical algorithms for satellite-derived sea surface temperatures, *Journal of Geophysical Research*, 94(D3):3365–3375.
- Berk, A., G.P. Anderson, P.K. Acharya, L.S. Bernstein, L. Muratov, J. Lee, M. Fox, S.M. Adler-Golden, J.H. Chetwynd, M.L. Hoke, R.B. Lockwood, J.A. Gardner, T.W. Cooley, C.C. Borel, P.E. Lewis, and E.P. Shettle, 2006. MODTRAN5: 2006 Update, *Proceedings of SPIE*, 6233:62331F.
- Birkenheuer, D.J., 1991. An algorithm for operational water vapor analyses integrating GOES and dual-channel microwave radiometer data on the local scale, *Journal of Applied Meteorology*, 30(6):834–843.
- Bolgren, D.W., N.G. Granin, and L. Levin, 1995. Surface temperature dynamics of Lake Baikal observed from AVHRR images, *Photogrammetric Engineering & Remote Sensing*, 61(2):211–216.
- Cavaliere, D.J., 1984. Determination of sea ice parameters with the NIMBUS 7 SMMR, *Journal of Geophysical Research*, 89 (D4): 5355–5369.
- Cavaliere, D.J., 1994. A microwave technique for mapping thin sea ice, *Journal of Geophysical Research*, 99(C6):12561–12572.
- Chesters, D., L.W. Uccellini, and W.D. Robinson, 1983. Low level water vapor fields from the VISSR atmospheric sounder (VAS) split window channels, *Journal of Applied Meteorology*, 22(5):725–743.
- Ciappa, A., L. Pietranera, and G. Budillon, 2012. Observations of the Terra Nova Bay (Antarctica) polynya by MODIS ice surface temperature imagery from 2005 to 2010, *Remote Sensing of Environment*, 119:158–172.
- Coll, C., V. Caselies, A. Sobrino, and E. Valor, 1994. On the atmospheric dependence of the split-window equation for land surface temperature, *International Journal of Remote Sensing*, 15(1):105–122.
- Comiso, J.C., 1994. Surface temperatures in the polar regions from Nimbus-7 temperature humidity infrared radiometer, *Journal of Geophysical Research: Oceans*, 99(C3):5181–5200.
- Franca, G.B., and A.P. Cracknell, 1994. Retrieval of land and sea surface temperature using NOAA-11 AVHRR data in northeastern Brazil, *International Journal of Remote Sensing*, 15(8):1695–1712.
- Frey, R., S. Ackerman, Y. Liu, K. Strabala, H. Zhang, J. Key, and X. Wang, 2008. Cloud detection with MODIS - Part I: Improvements in the MODIS cloud mask for collection 5, *Journal of Atmospheric and Oceanic Technology*, 25(7):1057–1072.
- Genthon, C., D. Six, V. Favier, M. Lazzara, and L. Keller, 2011. Atmospheric temperature measurement biases on the Antarctic plateau, *Journal of Atmospheric and Oceanic Technology*, 28(12):1598–1605.
- Germain, K.M.St., and D.J. Cavaliere, 1997. A microwave technique for mapping ice temperature in the Arctic seasonal sea ice zone, *IEEE Transactions on Geoscience and Remote Sensing*, 35(4):946–953.
- Hall, D.K., J.R. Key, K.A. Casey, G.A. Riggs, and D.J. Cavaliere, 2004. Sea ice surface temperature product from MODIS, *IEEE Transactions on Geoscience and Remote Sensing*, 42(5):1076–1087.
- Hall, D.K., R.S. Williams, K.A. Casey, N.E. DiGirolamo, and Z. Wan, 2006. Satellite-derived, melt-season surface temperature of the Greenland Ice Sheet (2000 - 2005) and its relationship to mass balance, *Geophysical Research Letters*, 33(11):L11501.
- Hall, D.K., J.E. Box, K.A. Casey, S.J. Hook, C.A. Shuman, and K. Steffen, 2008. Comparison of satellite-derived and in situ observations of ice and snow surface temperatures over Greenland, *Remote Sensing of Environment*, 112(10):3739–3749.
- Hall, D.K., J.C. Comiso, N.E. Digirolamo, C.A. Shuman, J.R. Key, and L. Koenig, 2012. A satellite-derived climate-quality data record of the clear-sky surface temperature of the Greenland Ice Sheet, *Journal of Climate*, 25(14):4785–4798.
- Hall, D.K., J.C. Comiso, N.E. Digirolamo, C.A. Shuman, J.E. Box, and L.S. Koenig, 2013. Variability in the surface temperature and melt extent of the Greenland ice sheet from MODIS, *Geophysical Research Letters*, 40:2114–2120.
- Harvey, J.W., and E.J. Green, 2013. Illustrating the temporal progress of environmental change, *Photogrammetric Engineering & Remote Sensing*, 79(12):1159–1170.
- Hori, M., T. Aoki, T. Tanikawa, H. Motoyoshi, A. Hachikubo, K. Sugiura, T.J. Yasunari, H. Eide, R. Storvold, Y. Nakajima, and F. Takahashi, 2006. In situ measured spectral directional emissivity of snow and ice in the 8 - 14 μm atmospheric window, *Remote Sensing of Environment*, 100(4):486–502.
- Hudson, S.R., and R.E. Brandt, 2005. A look at the surface-based temperature inversion on the Antarctic Plateau, *Journal of Climate*, 18(11):1673–1696.
- Hwang B.J., and D.G. Barber, 2008. On the impact of ice emissivity on sea ice temperature retrieval using passive microwave radiance data, *IEEE Geoscience and Remote Sensing Letters*, 5(3):448–452.
- Jimenez-Munoz, J.C., J.A. Sobrino, D. Skokovic, C. Mattar, and J. Cristobal, 2014. Land surface temperature retrieval methods from Landsat-8 thermal infrared sensor data, *IEEE Transactions on Geoscience and Remote Sensing*, 11(10):1840–1843.
- Kaufman, Y.J., and B.C. Gao, 1992. Remote sensing of water vapor in the Near IR from EOS/MODIS, *IEEE Transactions on Geoscience and Remote Sensing*, 30(5):871–884.
- Key, J., and M. Haeffliger, 1992. Arctic ice surface temperature retrieval from AVHRR thermal channels, *Journal of Geophysical Research*, 97(D5):5885–5893.
- Key, J.R., J.B. Collins, C. Fowler, and R.S. Stone, 1997. High-latitude surface temperature estimates from thermal satellite data, *Remote Sensing of Environment*, 61(2):302–309.
- Kleespies, T.J., and L.M. McMillin, 1990. Retrieval of precipitable water from observations in the split window over varying surface temperatures, *Journal of Applied Meteorology*, 29(9):851–862.
- Koenig L.S., and D.K. Hall, 2010. Comparison of satellite, thermochron and air temperatures at Summit, Greenland, during the winter of 2008/09, *Journal of Glaciology*, 56(198):735–741.
- Lazzara, M.A., G.A. Weidner, L.M. Keller, J.E. Thom, and J.J. Cassano, 2012. Antarctic automatic weather station program: 30 years of polar observation, *American Meteorological Society*, 93(10):1519–1537.
- Leshkevich, G.A., D.J. Schwab, and G.C. Muhr, 1993. Satellite environmental monitoring of the Great Lakes: A review of NOAA's Great Lakes CoastWatch program, *Photogrammetric Engineering & Remote Sensing*, 59:371–380.
- Liu, Y., J. Key, R. Frey, S. Ackerman, and W. Menzel, 2004. Nighttime polar cloud detection with MODIS, *Remote Sensing of Environment*, 92(2):181–194.
- Liu, Y., J.R. Key, and X. Wang, 2009. Influence of changes in sea ice concentration and cloud cover on recent Arctic surface temperature trends, *Geophysical Research Letters*, 36(20):L20710.
- Liu, Y., S. Ackerman, B. Maddux, J. Key, and R. Frey, 2010. Errors in cloud detection over the Arctic using a satellite imagery and implications for observing feedback mechanisms, *Journal of Climate*, 23(7):1894–1907.
- Mao, K., Z. Qin, J. Shi, and P. Gong, 2005. A practical split-window algorithm for retrieving land surface temperature from MODIS data, *International Journal of Remote Sensing*, 26(15):3181–3204.
- Marks, R.D., 2002. Astronomical seeing from the summits of the Antarctic plateau, *Astronomy & Astrophysics*, 385(1):328–336.
- McClain, E.P., W.G. Pichel, and C.C. Walton, 1985. Comparative performance of AVHRR-based multichannel sea surface temperatures, *Journal of Geophysical Research*, 90(C6):11587–11601.

- Mcfarland, M.J., R.J. Miller, and M. Christopher, 1990. Land surface temperature derived from the SSM/I passive microwave brightness temperature, *IEEE Transactions on Geoscience and Remote Sensing*, 28(5):839–845.
- McMillin, L.M., 1975. Estimation of sea surface temperature from two infrared window measurements with different absorptions, *Journal of Geophysical Research*, 80:5113–5117.
- Miller, D.H., 1956. The influence of snow cover on local climate in Greenland, *Journal of Meteorology*, 13(1):112–120.
- Nichol, J., 2009. An emissivity modulation method for spatial enhancement of thermal satellite images in urban heat island analysis, *Photogrammetric Engineering & Remote Sensing*, 75(5):547–556.
- Niclòs, R., V. Caselles, C. Coll, and E. Valor, 2007. Determination of sea surface temperature at large observation angles using an angular and emissivity-dependent split-window equation, *Remote Sensing of Environment*, 111(1):107–121.
- Ouaidrari, H., S.N. Goward, K.P. Czajkowski, J.A. Sobrino, and E. Vermote, 2002. Land surface temperature estimation from AVHRR thermal infrared measurements, An assessment for the AVHRR land Pathfinder II data set, *Remote Sensing of Environment*, 81(1):114–128.
- Peña, M.A., 2009. Examination of the land surface temperature response for Santiago, Chile, *Photogrammetric Engineering & Remote Sensing*, 75(10):1191–1200.
- Peter, U.C., B.A. Richard, and P. David, 1999. Northern hemisphere ice-sheet influences on global climate change, *Science*, 286(5442):1104–1111.
- Price, J.C., 1984. Land surface temperature measurements from the split window channels of the NOAA-7 advanced very high resolution radiometer, *Journal of Geophysical Research*, 89(D5): 231–237.
- Qin, Z., G.D. Olmo, and A. Karnieli, 2001. Derivation of split window algorithm and its sensitivity analysis for retrieving land surface temperature from NOAA advanced very high resolution radiometer data, *Geophysical Research*, 106(D19):22655–22670.
- Rajasekar, U., and Q. Weng, 2009. Application of association rule mining for exploring the relationship between urban land surface temperature and biophysical/social parameters, *Photogrammetric Engineering & Remote Sensing*, 75(4):385–396.
- Salisbury, J.W., D.M. D’Aria, and A. Wald, 1994. Measurements of thermal infrared spectral reflectance of frost, snow, and ice, *Journal of Geophysical Research*, 99(B12):24235–24240.
- Shu, Q., F. Qiao, Z. Song, and C. Wang, 2012. Sea ice trends in the Antarctic and their relationship to surface air temperature during 1979 - 2009, *Climate Dynamics*, 38(11-12):1–9.
- Shuman, C.A., D.K. Hall, N.E. Digirolamo, T.K. Mefford, and M.J. Schnaubelt, 2014. Comparison of near-surface air temperatures and MODIS ice surface temperatures at Summit, Greenland (2008-13), *Journal of Applied Meteorology and Climatology*, 53(9):2171–2180.
- Steffen, K., J.E. Box, and W. Abdalati, 1996. Greenland climate network: GC-Net, *US Army Cold Regions Research and Engineering (CRREL)*, pp. 98–103.
- Stroeve, J., M. Haeffliger, and K. Steffen, 1996. Surface temperature from ERS-1 ATSR infrared thermal satellite data in polar regions, *Journal of Climate and Applied Meteorology*, 35(8):1231–1239.
- Sobota, I., 2011. Snow accumulation, melt, mass loss, and the near-surface ice temperature structure of Irenebreen, Svalbard, *Polar Science*, 5(3):327–336.
- Tang, B.H., Y. Bi, Z.L. Li, and J. Xia, 2008. Generalized split-window algorithm for estimate of land surface temperature from Chinese geostationary FengYun meteorological satellite (FY-2C) data, *Sensors*, 8(2):933–951.
- Thenkabail, P., P. GangadharaRao, T. Biggs, M. Krishna, and H. Turrall, 2007. Spectral matching techniques to determine historical land-use/land-cover (LULC) and irrigated areas using time-series 0.1-degree AVHRR Pathfinder datasets, *Photogrammetric Engineering & Remote Sensing*, 73(10):1029–1040.
- Veihelmann, B., F.S. Olesen, and C. Kottmeier, 2001. Sea ice surface temperature in the Weddell Sea (Antarctica) from drifting buoy and AVHRR data, *Cold Regions Science and Technology*, 33(1):19–27.
- Vincent, R.K., 2000. Forecasts of monthly averaged daily temperature highs in Bowling Green, Ohio from monthly sea surface temperature anomalies in the Eastern Pacific ocean during the previous year, *Photogrammetric Engineering & Remote Sensing*, 66(8):1001–1010.
- Wald, A., 1994. Modeling thermal infrared (2–14 μm) reflectance spectral of frost and snow, *Journal of Geophysical Research*, 99(24):241–24, 250.
- Wan, Z., D. Ng, and J. Dozier, 1994. Spectral emissivity measurements of land-surface materials and related radiative transfer simulations, *Advances in Space Research*, 14(3):91–94.
- Warren, S.G., 1982. Optical properties of snow, *Reviews of Geophysics and Space Physics*, 20(1):67–89.
- Wynne, R.H., and T.M. Lillesand, 1993. Satellite observation of lake ice as a climate indicator: Initial results from statewide monitoring in Wisconsin, *Photogrammetric Engineering & Remote Sensing*, 59(6):1023–1031.
- Xiao, R., Q. Weng, Z. Ouyang, W. Li, E.W. Schienke, and Z. Zhang, 2008. Land surface temperature variation and major factors in Beijing, China, *Photogrammetric Engineering & Remote Sensing*, 74(4):451–461.
- Zwally, H.J., W. Abdalati, T. Herring, K. Larson, J. Saba, and K. Steffen, 2002. Surface melt-induced acceleration of Greenland ice-sheet flow, *Science*, 297(5579):218–222.

(Received 20 October 2014; accepted 30 June 2015; final version 08 July 2015)